

# We are IntechOpen, the world's leading publisher of Open Access books Built by scientists, for scientists

6,900

Open access books available

186,000

International authors and editors

200M

Downloads

Our authors are among the

154

Countries delivered to

TOP 1%

most cited scientists

12.2%

Contributors from top 500 universities



WEB OF SCIENCE™

Selection of our books indexed in the Book Citation Index  
in Web of Science™ Core Collection (BKCI)

Interested in publishing with us?  
Contact [book.department@intechopen.com](mailto:book.department@intechopen.com)

Numbers displayed above are based on latest data collected.  
For more information visit [www.intechopen.com](http://www.intechopen.com)



# Using Metamaterial-Based Coplanar Waveguide Structures for the Design of Antennas on Passive UHF RFID Tags

Benjamin D. Braaten and Masud A. Aziz  
*North Dakota State University  
United States*

## 1. Introduction

Radio Frequency Identification (RFID) is becoming a very affordable and reliable way of to track inventory items. Because of this, RFID systems have received considerable attention from researchers, engineers and industry personnel. Particularly, researchers involved with RFID systems have developed smaller antennas for tags deployed in these systems. Several of these designs have involved meander-line antennas (Finkenzeller, 2003), metamaterial-based designs (Dacuna & Pous, 2007) and various materials (Griffin et. al., 2006). This chapter will describe the main parameters of interest in a RFID system using Friis's transmission equation. This will then be followed by a section on recent work on applying RFID systems to smart shelves, metallic plates and livestock tracking. Then a section on coplanar-waveguides (CPW) is presented followed by the design of metamaterial-based CPW antennas for passive UHF RFID tags.

## 2. An introduction to passive RFID systems

RFID technology is an automatic means of object identification with minimal human intervention or error (Qing & Chen, 2007). Recently, RFID technology has been extensively used to improve automation, inventory control, tracking of grocery products in the retail supply chain and management of large volumes of books in libraries (Jefflindsay, 2010; Teco, 2010). RFID tags have functions similar to a bar code; however they can be detected even when they are blocked by obstacles. RFID tags also carry more information than a bar code (Finkenzeller, 2003).

A RFID system consists of a reader (or interrogator) and several tags (or transponders). A typical RFID system is shown in Fig 1. The reader consists of a transmitting and receiving antenna and it is typically connected to a PC or any other monitoring device. The tag has a single antenna for both transmitting and receiving. Digital circuitry (or IC) that communicates with the reader is attached to the antenna on the tag. The reader sends out an electromagnetic field that contains power and timing information into the space around itself (sometimes called the interrogation zone (Finkenzeller, 2003)). If there is a tag in the interrogation zone, then the tag receives the electromagnetic field using its receiving antenna. The tag then utilizes its IC to communicate with the reader. The IC collects power

and timing information from the electromagnetic field and sends proper backscattered messages to the reader using the transmitting antenna of the tag. The maximum distance that a reader can interrogate a tag is termed as the max read range of the tag.

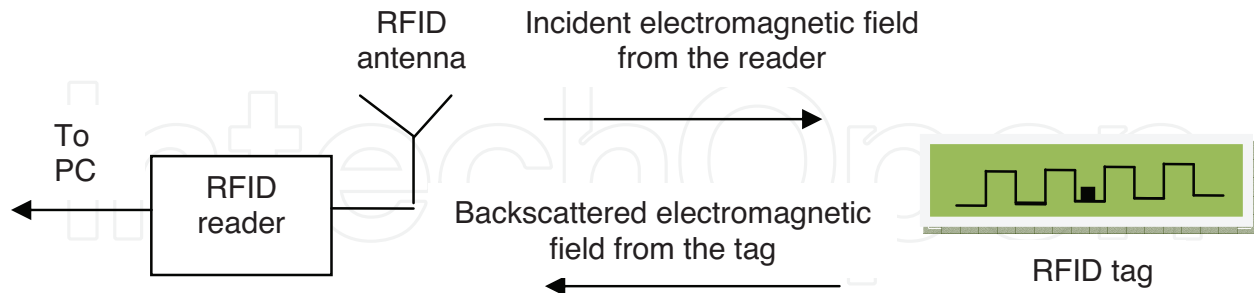


Fig. 1. Overview of a RFID system.

Depending upon the power source of the tag, a RFID system can be classified into three major categories: active, semi-passive, and passive (Finkenzeller, 2003). An active tag uses its own power from the battery attached to it to communicate with the reader. A semi-passive tag also has its own battery but it is only awakened by the incident electromagnetic field from the reader. This greatly enhances the read range of the tag (Finkenzeller, 2003). A passive tag uses the power from the incident electromagnetic field. The incoming electromagnetic field from the reader induces a port voltage on the tag antenna and the IC uses its power harvesting circuit to provide power to the digital portion of the circuit. The power is then used by the IC to communicate with the reader.

The RFID system can be described by the Friis transmission equation (Stutzman & Thiele, 1998):

$$P_r = P_t \frac{G_r G_t \lambda^2}{(4\pi R)^2} q \quad (1)$$

where  $P_t$  is the power transmitted by the reader,  $P_r$  is the power received by the passive tag,  $G_t$  is the gain of the antenna on the reader,  $G_r$  is the gain of the antenna on the tag,  $\lambda$  is the free-space wavelength of the transmitting frequency by the reader,  $R$  is the distance between the antenna on the reader and the antenna on the tag and  $q$  is the impedance mismatch factor ( $0 \leq q \leq 1$ ) between the passive IC and the antenna.

Equation (1) assumes a polarization match between the antenna used by the reader and the antenna on the passive tag. Therefore, a good match between the passive IC and the antenna on the tag is essential. It is also assumed that the tag is in the far-field of the reader. Therefore, a larger gain of the antenna on the tag will mean more power for the passive IC on the tag. Moreover, using a longer wavelength will also improve the power at the tag. However, the power available to the tag reduces by the distance squared as the tag and reader antenna are moved apart. Equation (1) can also be expressed as follows (Braaten et al., 2008; Rao et al., 2005):

$$R = \frac{\lambda}{4\pi} \sqrt{\frac{q G_t G_r P_t}{P_r}} \quad (2)$$

If the threshold power required to activate the IC on the tag is  $P_{thr}$ , then maximum read range  $r_{max}$  can be derived from Equation (2)

$$r_{max} = \frac{\lambda}{4\pi} \sqrt{\frac{qG_t G_r P_t}{P_{th}}} . \quad (3)$$

Equation (3) is very useful for predicting the max read range of a passive RFID tag. Generally,  $P_{th}$  of a RFID tag is known. Moreover,  $P_t$  and  $G_t$  are fixed. This leaves the two variables  $q$  and  $G_r$  to the designer. Typically, a tag is designed to have the highest  $r_{max}$ . One way of achieving this is to have a good match between the antenna and the IC on the tag with a large  $G_r$ .

### 3. Summary of previous work

#### 3.1 RFID shelves

Recently, the RFID smart-shelf system has received considerable attention. This is due to the increasing demands for large-scale management of such items as grocery products in the retail supply chain, large volume of books in libraries, bottles in the pharmaceutical industry, and important documentation in offices (Landt, 2005; Want, 2006). The RFID smart shelf is a regular shelf with a reader antenna embedded in the shelf. This ideally allows for only detecting the tagged items located on that shelf. Extending this concept to every shelf in a store makes it possible to automatically locate and inventory every item.

There have been many different smart-shelves proposed by different authors. Design of a smart-shelf can be found in both the High Frequency (HF) and Ultra-High Frequency (UHF) range. The main difference is that at HF the energy coupling between the reader antenna and the tag is essentially made through the magnetic field (Medeiros et al., 2008). A very common reader antenna configuration is a loop antenna (Qing & Chen, 2007; Cai et. al., 2007). Good coupling requires close proximity between the reader antenna and the tag. At UHF, readers are equipped with antennas such as patch antennas (Lee et. al., 2005) and energy coupling to the tag antenna is made through propagating waves.

At UHF, it is difficult to limit the antenna radiation exactly to the shelf boundary without resorting to costly metal or absorbing shields. One solution can be to incorporate a leaking microstrip line with an extended ground plane in the shelf. This shelf design exploits the leaking fields from a microstrip line (undesirable in microwave circuits) for applications of RFID systems in small areas (Medeiros et al., 2008).

#### 3.2 Tags on metallic objects

There is a strong interest from many industries (aeronautics, automotive, construction, etc.) in tagging metal items (airplane or automotive parts, metal containers, etc.) using both active and passive RFID tags (Rao et. al., 2008). Unfortunately, tag performance is affected by the electrical properties of metal objects that are in contact or close proximity to the tag antenna. A series of measurements were used to measure the far-field gain pattern and gain penalty of several tag antennas when connected to different objects (Griffin et. al., 2006). The Antenna Gain Penalty (AGP) is defined to be the loss in gain of the antenna due to metal attachment. The measured gain showed sufficient distortion due to permittivity, loss tangent of the material, surface waves and diffraction (Griffin et. al., 2006).

The presence of the metal plate shifts up the resonant frequency of the HF reader loop antenna and weakens the intensity of the magnetic field (Qing & Chen, 2007). When a metal plate is positioned close to a loop antenna, the magnetic field generated by the loop antenna reaches the surface of the metal plate. In order to satisfy the boundary conditions on the

metal surface, the magnetic field normal to the surface must be zero. For this to occur, an additional current, known as the eddy current, is induced within the metal plate. The induced current opposes the magnetic flux generated by the antenna, which may significantly dampen the magnetic flux in the vicinity of the metal surface. The damping of magnetic flux leads to a reduction of the inductance of the loop antenna. Therefore, the resonant frequency of the antenna is increased (Finkenzeller, 2003). The resonant frequency of the antenna also depends on the position of the metal objects. The back-placed metal (metal positioned at the back of the antenna) has the most significant impact on the resonant frequency of the antenna as opposed to the side or bottom placed metal (Qing & Chen, 2007).

Several antennas have been proposed to overcome the abovementioned constraints. An RFID tag with a thin foam backing material that is capable of operating efficiently both as a dipole antenna and as a microstrip antenna has been proposed (Mohammed et. al., 2009). The antenna behaves as a dipole antenna in free space and acts as a patch antenna when it is attached to metal objects. A wideband metal mount RFID tag that works on a variety of metals also was proposed (Rao et. al., 2008). Reduction in the size of the antenna also has been achieved by introducing a quasi-Yagi antenna on a RFID tag (Zhu et. al., 2008). The impact of a wooden and metallic surface together on the antenna has also been studied (Kanan & Azizi, 2009).

### 3.3 Cattle tag research

RFID technology has many applications. One use of this technology is for livestock identification. Animals such as cattle and sheep are tagged for purposes, such as disease control, breeding management, and stock management (Ng et. al., 2005). Loop antennas have been proposed as the RFID tag antenna in the cattle tags (Braaten et. al., 2006). One of the reasons that loop antennas are widely used is that they are not required to be very large. Loops are used as receiving antennas because the output of the loop is proportional to the number of turns and the permeability of the material the loop is wound on. Therefore, weak signals can be detected by using a loop with a large number of turns and wound on a material with significant permeability. Antennas with dielectric superstrates have also been proposed (Braaten et. al., 2008). It has been shown that a passive tag with a meander-line antenna and dielectric superstrate can significantly augment the read range of the tag.

## 4. Coplanar-waveguide structures

Coplanar-waveguide (CPW) transmission lines are used extensively in wireless communications (Pozar, 2005; Collin, 2001). A CPW transmission line is shown in Fig. 2. The reference planes and signal plane are printed on the same conducting layer. Each plane is usually made of a conducting material such as copper. The dielectric is typically isotropic and ungrounded. The signal propagating down the CPW transmission line is symmetrically guided between the signal plane and the outer reference planes. The advantages of a CPW transmission line are that it only requires a single conducting layer and components can be easily connected between the signal plane and the reference plane. This is very useful for printed circuit boards with many different layers because only a single layer dedicated to microwave signals is needed. The disadvantage of a CPW transmission line is the need to keep both reference planes at the same potential all along the signal trace. This can be difficult to do on a single conducting layer.

Many advances have been made on the CPW transmission line. For example novel filters have been developed (Velez et al., 2009) and right/left-handed propagation has been demonstrated (Eleftheriades and Balmain, 2005) on CPW transmission lines. Many of the new techniques and structures that have been developed can also be used for the design of new antennas. The following section uses a new structure developed for CPW filters to reduce the overall size of printed dipoles.

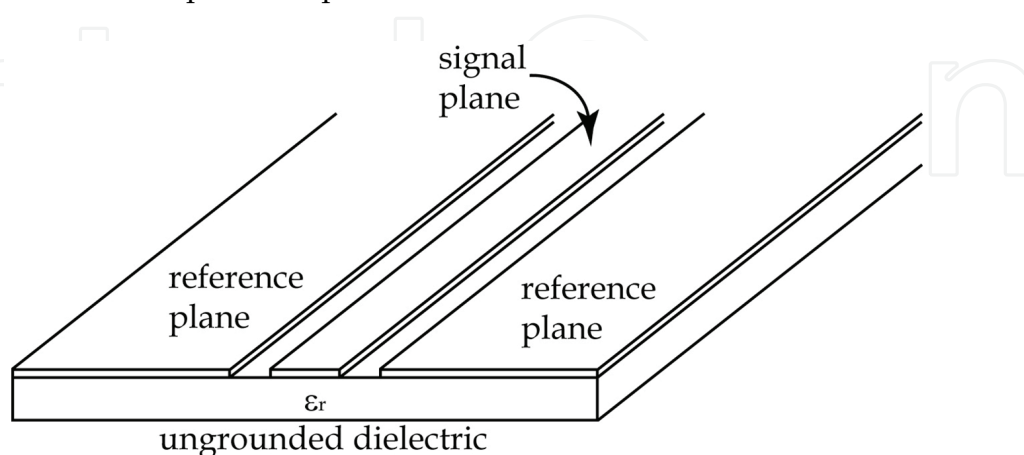


Fig. 2. A CPW transmission line on a dielectric substrate.

## 5. Metamaterial-based antenna design using OCSRR and MOCSRR particles.

Antennas on a passive UHF RFID tag are typically printed on the top side of a thin flexible substrate while adhesive is applied to the bottom side to attach the tag to a desired object. Because of this, all the conducting material (i.e., copper) used for the antenna is constrained to a single layer. This restriction requires the entire topology of the antenna to be printed on the same plane. Many different types of meander-line antennas for passive UHF RFID tags printed on a single conducting layer have been proposed (Marrocco, 2003; Calabrese et al., 2008). Many of these meander-line antennas have proven to be useful, however recently a special type of printed dipole (Braaten, 2010a; Braaten et al., 2010b) based on the meander-line structure has recently been developed. Particularly, these newly developed printed antennas use open complementary split ring resonator (OCSRR) and meander open complementary split ring resonator (MOCSRR) particles connected in series to form electrically small resonant dipoles (Velez et al., 2009).

### 5.1 The OCSRR particle

First, the OCSRR particle is introduced. The layout of each individual OCSRR particle is shown in Fig. 3 (a). Each particle is a coplanar-waveguide (CPW) structure with various concentric ring gaps etched from the copper. A port is defined on each side of the particle and the equivalent circuit in Fig. 3 (b) is used to model the OCSRR particle in Fig. 3 (a). The equivalent inductance  $L_{eq,o}$  represents the inductance between ports a and b caused by the ring between the ring slots connecting the two ports and the equivalent capacitance  $C_{eq,o}$  represents the distributed capacitance between ports a and b caused by the ring slots. Each section of the meander-line antenna in Fig. 4 has the same equivalent circuit as the OCSRR particle in Fig. 3 (b). Therefore, by connecting several OCSRR particles in series, an alternate electrically small resonant antenna can be designed.

## 5.2 Equivalent circuit and the dimensional relation of the OCSRR particle

To illustrate the behaviour of the OCSRR particle in Fig. 3, the equivalent circuit is extracted and discussed in this section for various values of  $r_d$  (i.e., inner disc radius values) of the OCSRR particle. The CPW structure shown in Fig. 5 can be used to extract the equivalent circuit of the OCSRR particle (Velez et al., 2009). A convenient method of extracting the equivalent circuit is to use a commercially available full wave electromagnetic solver such as Momentum (Advanced Design System 2009a) to simulate the CPW structure in Fig. 5. When the particles resonate, the impedance on the 50  $\Omega$  CPW transmission line caused by the particles is infinity. This will result in an optimum match (i.e., lowest  $S_{11}$  values) between the 50  $\Omega$  ports and 50  $\Omega$  CPW transmission line to occur at resonance. Then, from the simulated  $S_{11}$  values, an equivalent circuit can be extracted using a curve fitting technique. This equivalent circuit can then be placed in the location of the OCSRR particle in Fig. 3 and be used to represent the physical OCSRR particle. The equivalent circuit loads the 50  $\Omega$  CPW transmission line in a manner similar to the actual OCSRR particles. With a technique to extract the equivalent circuit of the OCSRR particle, a designer is able to determine how various dimensions of the OCSRR particle ultimately affect the equivalent circuit of that particular particle. Particularly, how the dimensions affect the individual capacitance and inductance values of the equivalent circuit of the OCSRR particle can be shown.

Using the method described in the previous paragraph, the equivalent circuit of the OCSRR particle in Fig. 3 (a) was extracted for various dimensions of the inner disc (i.e., for various values of  $r_d$ ) and scale factors (i.e., for various values of  $S$ ). For the various values of  $r_d$  the dimensions of the OCSRR particle were  $w = 8.3$  mm,  $h = 8.1$  mm,  $s = 0.51$  mm,  $m = 0.47$  mm,  $n = 0.39$  mm,  $r_i = 0.45$  mm and  $t = 0.39$  mm. The substrate was defined to be 1.36 mm thick and had a permittivity of 4.2. The values of  $M$  and  $N$  in Fig. 5 are 0.4 mm and 3.1 mm, respectively. The results from these computations are shown in Table 1. The results in Table 1 can be used to design an OCSRR particle with a specific resonant frequency.

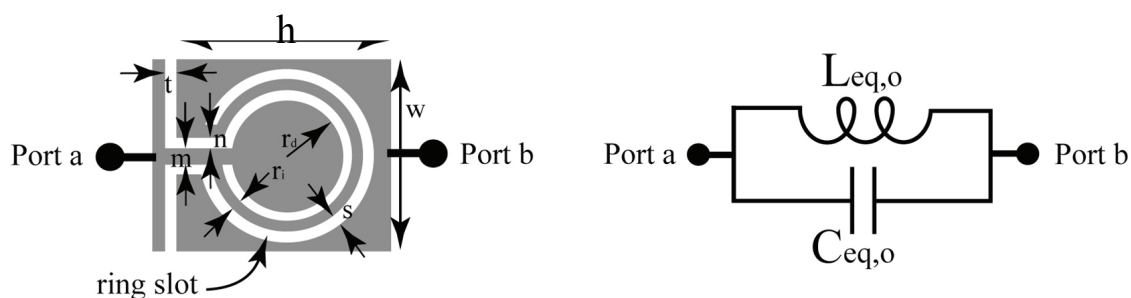


Fig. 3. (a) Layout of the OCSRR particle (the gray area is the copper) and (b) the equivalent circuit of the OCSRR particle.

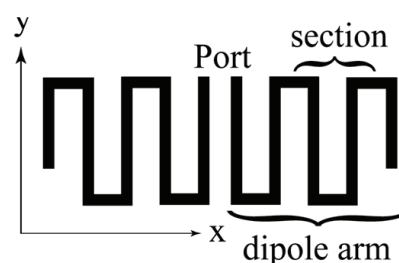


Fig. 4. Layout of a meander-line dipole.

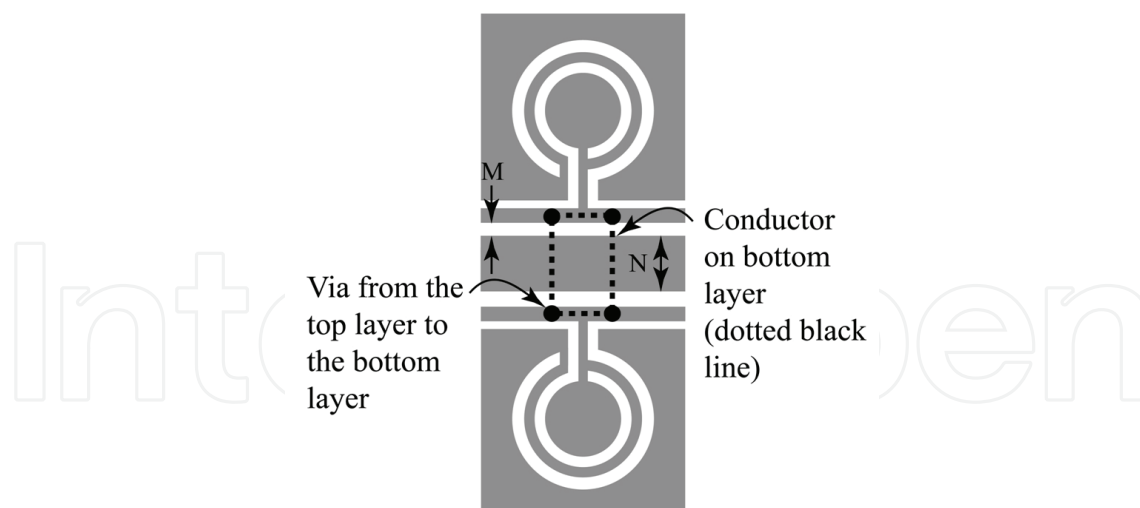


Fig. 5. CPW structure used to extract the equivalent circuit of the OCSRR particle (the gray area is the copper).

$r_d$ (mm)	$L_{eq}$ (nH)	$C_{eq}$ (pF)	$f_0$ (GHz)
1.0	1.5	2.95	2.39
1.2	1.5	2.95	2.39
1.4	1.5	3.0	2.37
1.6	1.5	3.0	2.37
1.8	1.4	3.25	2.35
2.0	1.7	3.05	2.2
2.2	1.7	3.05	2.2

Table 1. Equivalent circuit design table for the OCSRR particle for various values of  $r_d$ .

S	$L_{eq}$ (nH)	$C_{eq}$ (pF)	$f_0$ (GHz)
0.7	1.0	2.85	2.98
0.75	1.1	2.9	2.81
0.8	1.3	2.85	2.61
0.85	1.2	3.2	2.56
0.9	1.4	3.15	2.39
0.95	1.4	3.25	2.35
1.0	1.7	3.05	2.2

Table 2. Equivalent circuit design table for the OCSRR particle for various scale factors S.

Next, the dimensions of OCSRR particle were fixed at  $w = 8.3$  mm,  $h = 8.1$  mm,  $s = 0.51$  mm,  $m = 0.47$  mm,  $n = 0.39$  mm,  $r_i = 0.45$  mm,  $r_d = 2.0$  mm and  $t = 0.39$  mm. Starting from these dimensions the particles were scaled by several factors symmetrically in both the x- and y-directions. For example, for a scaling factor of  $S = 1.0$ , the dimensions of the particle are unchanged. Then by scaling the particle by 0.8, every dimension of the particle is reduced by

20%. A scaling factor of 0.7 then reduces the size of the particle by 30% and so on. The equivalent circuit and resonant frequency was computed for each scaling factor using the CPW structure in Fig. 5. The results from these computations are shown in Table 2.

### 5.3 Discussion

The results in Table 1 show how the resonant frequency of the OCSRR particle can be reduced by increasing the radius value of the inner disc. This is expected, because the equivalent capacitance of the particle is larger for larger radius values. The increased capacitance is a result of the smaller ring gap. As the distance between the conducting inner disk and the conducting ring (in the ring gap) reduces, the capacitance between the two conductors increase which results in a lower resonant frequency.

The results in Table 2 show how the resonant frequency is related to different scaling factors of the OCSRR particle. The resonant frequency of the particle was increased by approximately 6 – 7% for a 5% change in the scaling factor. This is very useful for designing an OCSRR particle for a specific resonant frequency.

### 5.4 Antenna designs using the OCSRR particle

OCSRR particles can be connected in series in a manner shown in Fig. 6 to form an electrically small resonant dipole. In fact, a dipole consisting of series connected OCSRR particles have characteristics similar to the meander-line dipole in Fig. 4. The equivalent circuit of each meander-line section is a capacitor connected in parallel with an inductor. The vertical traces in each meander-line section contribute to the equivalent capacitance and the current travelling on each horizontal segment contributes to the equivalent inductance. The equivalent circuit of an OCSRR particle is the same as the equivalent circuit of each meander-line section. Therefore, by connected OCSRR particles in series, an alternate to the meander-line dipole can be designed. Furthermore, it turns out that the overall size of a dipole with series connected OCSRR particles is much smaller than a meander-line dipole with the same resonant frequency.

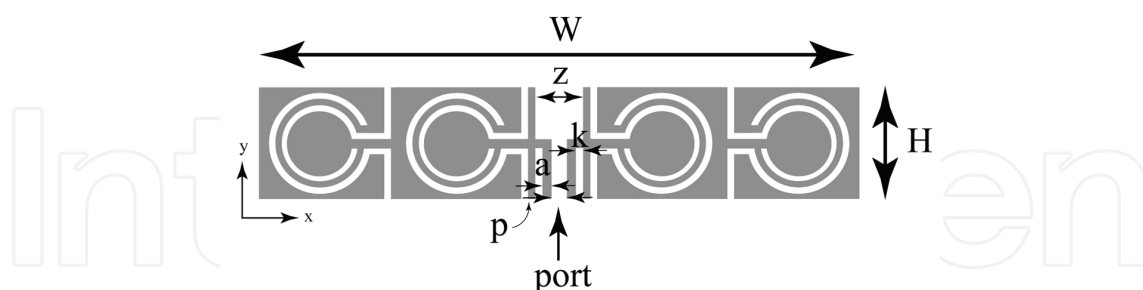


Fig. 6. Layout of the printed dipole using series connected OCSRR particles (the gray area is the copper).

The characteristics of the OCSRR dipole in Fig. 6 have been previously studied (Braaten, 2010a) and the results are summarized here in Tables 3 and 4. Table 3 shows how the input impedance of the OCSRR antenna in Fig. 6 changes for various values of  $\epsilon$  at a frequency of 920 MHz. The results in Table 4 show how the input impedance changes for various values of  $d$  (i.e., substrate thickness) at a frequency of 920 MHz. Using the results in Tables 3 and 4, a designer will be able to predict how the input impedance of the antenna on the tag may change by being attached to a particular item. Knowing this information is useful for

designing a successful antenna on a passive UHF RFID tag. Notice that the gain is mostly unaffected except for thicker substrates.

A prototype passive UHF RFID tag using the OCSRR antenna in Fig. 6 has also been presented and tested (Braaten, 2010a). The read range of the prototype tag was  $> 5$  m with overall dimensions of  $W = 55.54$  mm and  $H = 11.91$  mm. These overall dimensions are much smaller than many commercially available tags.

$\epsilon$	$f_0$ (MHz)	$Z_{in}$ ( $\Omega$ )	$G$ (dB)
1.0	920	6.6-j94.7	1.82
2.2	920	7.9-j27	1.89
4.25	920	13.8+j110	1.89
5.8	920	36.5+j375	1.76

Table 3. Input impedance and gain of the OCSRR antenna at 920 MHz for various values of  $\epsilon$ .

$d$ (mm)	$f_0$ (MHz)	$Z_{in}$ ( $\Omega$ )	$G$ (dB)
0.127	920	7.4-j49	1.87
0.787	920	13.8+j110	1.88
1.57	920	28.1+j288	1.70
3.14	920	93+j677	1.35

Table 4. Input impedance and gain of the OCSRR antenna at 920 MHz for various values of  $d$ .

### 5.5 The MOCSRR particle

Next, the characteristics of the MOCSRR particle are investigated. The layout of an individual MOCSRR particle is shown in Fig. 7 (a). This particle is similar to the OCSRR particle except the ring slots take a meander route between ports a and b and not a circular route as in the OCSRR particle. This meander route results in a much lower resonant frequency for over all dimensions similar to an OCSRR particle. This lower resonant frequency is very useful for designing small resonant dipoles which is important for designing small efficient passive RFID tags.

### 5.6 Equivalent circuit and the dimensional relation of the MOCSRR particle

Using the CPW structure in Fig. 8 and the method discussed in section 5.2, the equivalent circuit is extracted for the MOCSRR particle for various values of  $\delta$  and scaling factors. The dimensions of the MOCSRR particle in Fig. 7 are  $y = 8.2$  mm,  $x = 8.05$  mm,  $c = 0.42$  mm,  $v = 0.22$  mm,  $d = 2.92$  mm,  $h = 5.17$  mm,  $t = 0.33$  mm,  $g = 0.31$  mm and  $q = 0.43$  mm. The substrate was defined to have a thickness of 1.36 mm and a permittivity of 4.2. The values of  $M$  and  $N$  in Fig. 8 were 0.4 mm and 3.1 mm, respectively. The overall dimensions of the MOCSRR particle and the OCSRR particle are similar to show the differences between the equivalent circuits of each particle.

The results of these computations are shown in Tables 5 and 6. Table 5 shows how the resonant frequency can be reduced by increasing the value of  $\delta$  while the results in Table 6 show how the resonant frequency of the MOCSRR particle is related to the scaling factor

and  $\delta = 1.54$  mm. For a 5% reduction in the overall size of the particle, a 100 MHz increase in resonant frequency has been observed (i.e., the resonant frequency is approximately reduced 5 – 6% for each scale step).

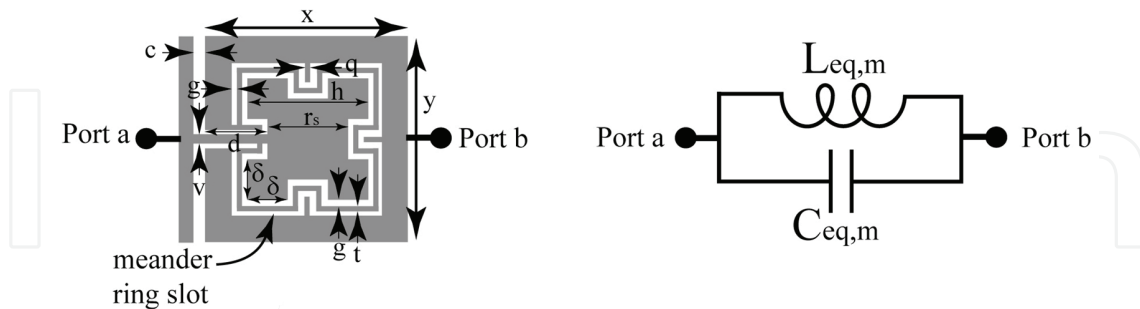


Fig. 7. (a) Layout of the MOCSRR particle (the gray area is the copper) and (b) the equivalent circuit of the MOCSRR particle.

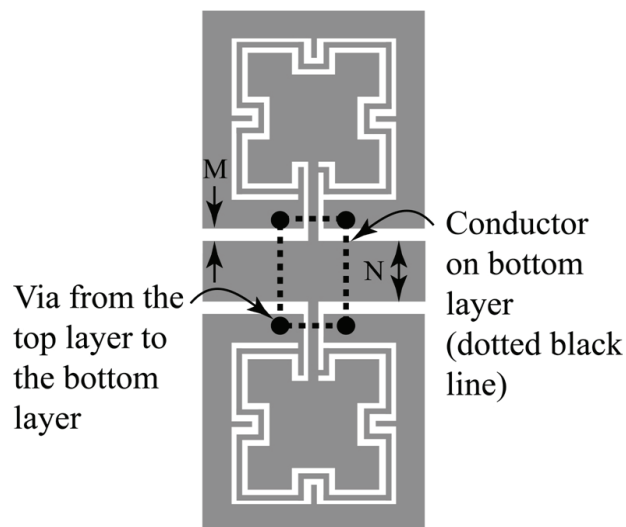


Fig. 8. CPW structure used to extract the equivalent circuit of the OCSRR particle (the gray area is the copper).

$\delta$ (mm)	$r_s$ (mm)	$L_{eq}$ (nH)	$C_{eq}$ (pF)	$f_0$ (GHz)
0.9	1.6	3.6	2.9	1.55
1.0	1.7	3.8	2.75	1.55
1.1	1.8	3.7	2.85	1.55
1.2	1.9	3.4	3.1	1.55
1.3	2.0	3.4	3.15	1.53
1.4	2.1	3.5	3.1	1.52
1.5	2.2	3.7	3.25	1.45

Table 5. Equivalent circuit design table for the MOCSRR particle for various values of dimension  $r_s$  and  $\delta$ .

S	$L_{eq}$ (nH)	$C_{eq}$ (pF)	$f_0$ (GHz)
0.7	2.4	2.25	2.16
0.75	2.7	2.45	1.95
0.8	2.9	2.6	1.83
0.85	2.9	2.9	1.73
0.9	3.2	2.95	1.63
0.95	3.4	3.1	1.55
1.0	3.7	3.25	1.45

Table 6. Equivalent circuit design table for the MOCSRR particle for various scale factors S.

### 5.7 Discussion

Comparing the results in Table 1 to the results in Table 5 shows how much the resonant frequency of the particle is reduced by using a meander ring slot instead of a circular ring slot. This is because the results in Tables 1, 2, 5 and 6 show that the MOCSRR particle has approximately twice the inductance as the OCSRR particle while the capacitance is comparable. This is very useful for antenna miniaturization because the impedance of the particles is inductive. This inductive property can be used for matching transmission lines to the capacitive input impedance of electrically small antennas.

### 5.8 Antenna designs using the MOCSRR particle

MOCSRR particles can be connected in a similar manner to the series connected OCSRR particles shown in Fig. 6 in section 5.4. This will result in the layout show in Fig. 9. Since the equivalent circuit of each MOCSRR particle has the same equivalent circuit of each meander-line section in Fig. 4, an electrically small resonant dipole can be designed.

To understand the behaviour of the antenna in Fig. 9, the input impedance was computed for various substrate values of permittivity and thicknesses. The results for  $a = 0.4$  mm and  $z = 1.09$  mm are shown in Figs. 10 - 13 (particle dimensions are defined in section 5.6 with  $\delta = 1.54$  mm).

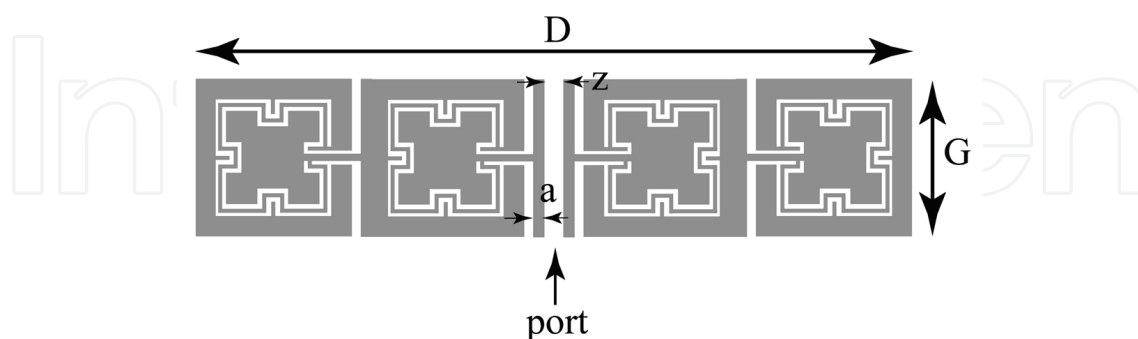


Fig. 9. Layout of the printed dipole using series connected MOCSRR particles (the gray area is the copper).

The results Figs. 10 and 11 show how the input impedance of the antenna is related to the permittivity of the substrate. For these computations the substrate thickness was fixed at  $d = 1.36$  mm. For example, at 920 MHz the antenna is most appropriately matched to the input impedance of the passive IC for a substrate permittivity of 4.2. This makes the antenna

in Fig. 9 desirable for printing on FR4 substrates. Figs. 10 and 11 also show how the input impedance can change dramatically for slightly lower and higher values of substrate permittivity. This information is useful for a designer when a tag is placed on various items. By understanding how the impedance of the antenna changes for various substrates, the maximum read range of a tag used on multiple items could be predicted.

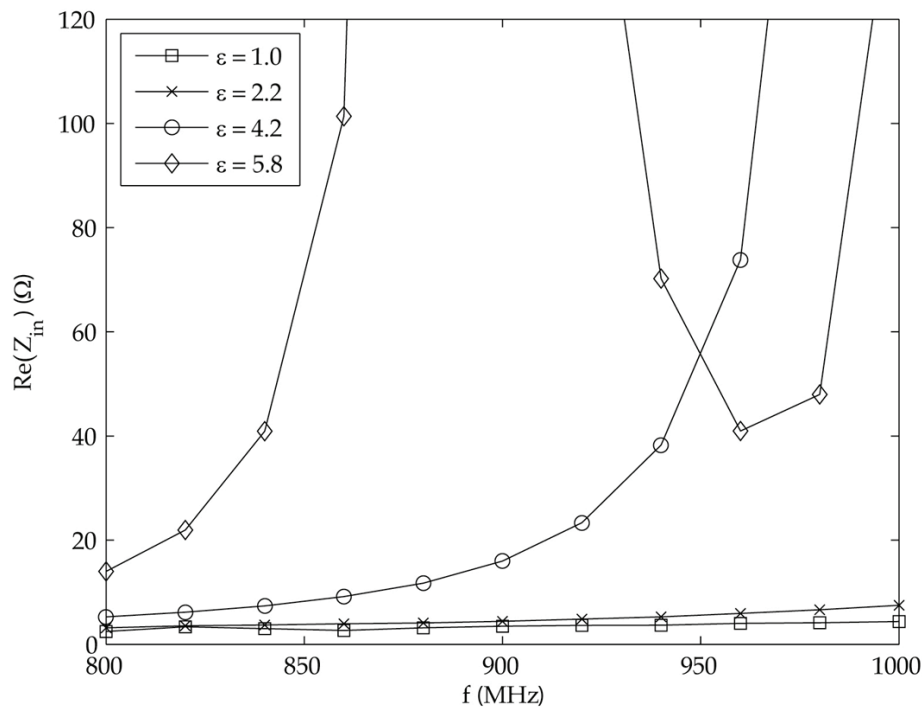


Fig. 10. Real part of the input impedance of the MOCSRR antenna for various values of  $\epsilon$ .

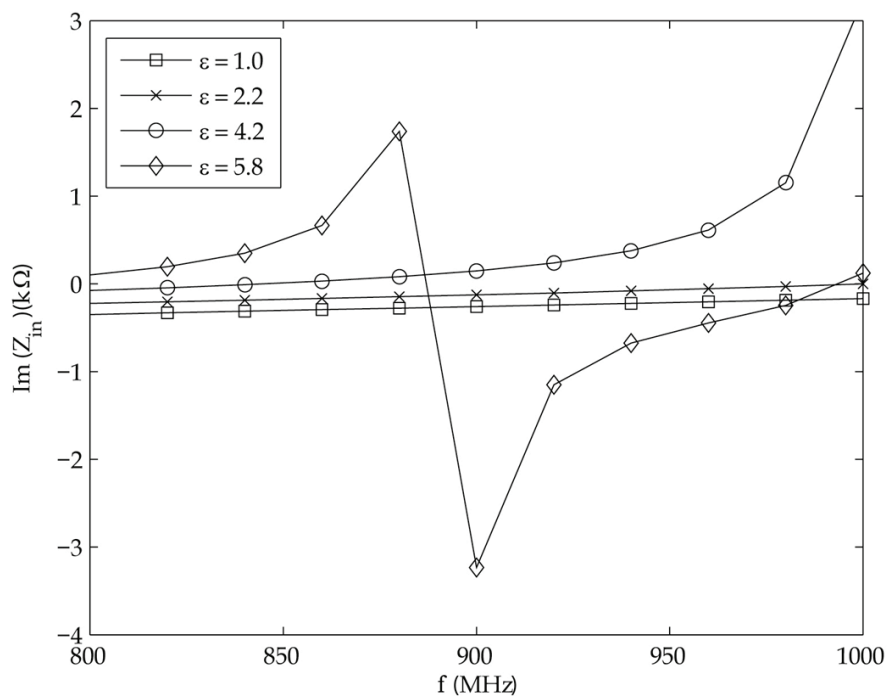


Fig. 11. Imaginary part of the input impedance of the MOCSRR antenna for various values of  $\epsilon$ .

The results in Figs. 12 and 13 provide further information on the behaviour of the MOCSRR antenna. These results show how the input impedance changes with substrates of different thicknesses. At 920 MHz the antenna in Fig. 9 has the optimum match at  $d = 1.36$  mm.

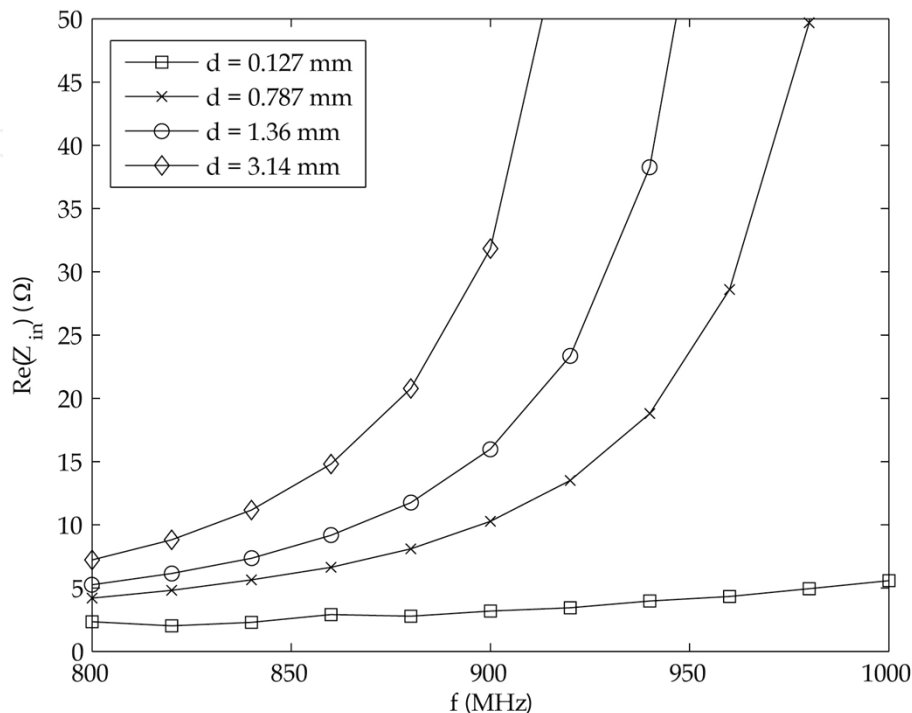


Fig. 12. Real part of the input impedance of the MOCSRR antenna for various values of  $d$ .

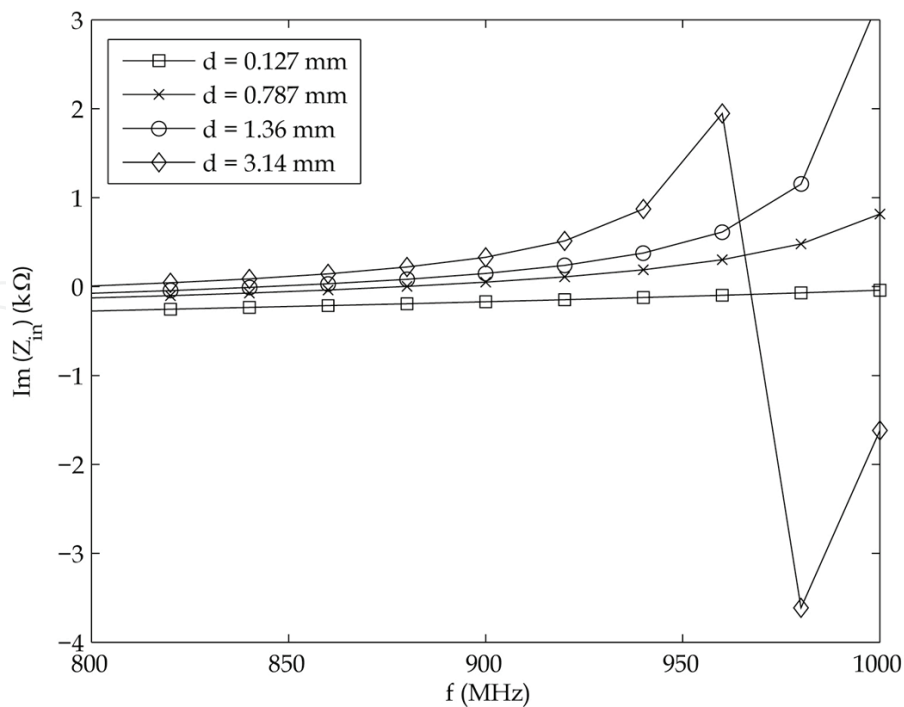


Fig. 13. Imaginary part of the input impedance of the MOCSRR antenna for various values of  $d$ .

## 6. Future work

Many different future topics of research could be explored as a result of this work. Several of these topics could involve work on a different type of CPW particle, left-handed propagation using the MOCSRR particles or analytical relations between the resonant frequencies of the particle to various geometrical values. Studying these topics could further reduce the size of the resonant antennas presented here or significantly shorten the design time for an engineer using these particular antennas on a passive RFID tag.

## 7. Conclusion

Initially in this work a RFID system has been introduced using the Friis transmission equation. This introduction was then followed by recent applications of RFID systems and an introduction of the CPW structure. This then lead to sections outlining the design of small resonant dipoles with OCSRR and MOCSRR particles. Particularly, the results in these sections showed how the resonant frequencies of the particles were extracted and related to various geometrical dimensions and how the input impedance of the small resonant dipoles was related to various substrates.

## 8. References

- Advanced Design System 2009a, Agilent Technologies, [www.agilent.com](http://www.agilent.com).
- Braaten, B.D.; Feng, Y.; & Nelson, R.M., "High-frequency RFID tags: an analytical and numerical approach for determining the induced currents and scattered fields," *IEEE International Symposium on Electromagnetic Compatibility*, pp. 58-62, August 2006, Portland, OR.
- Braaten, B. D.; Owen, G. J.; Vaselaar, D.; Nelson, R. M.; Bauer-Reich, C.; Glower, J.; Morlock, B; Reich, M.; & Reinholz, A., "A printed Rampart-line antenna with a dielectric superstrate for UHF RFID applications," in *Proceedings of the IEEE International Conference on RFID*, pp. 74-80, April, 2008, Las Vegas, NV.
- Braaten, B. D., "A novel compact UHF RFID tag antenna designed with series connected open complementary split ring resonator (OCSRR) particles," *IEEE Transactions on Antennas and Propagation*, vol. 58, no. 11, November, 2010a, pp. 3728 - 3733 2010a.
- Braaten, B. D.; Aziz, M. A.; Schroeder, M. J.; and Li, H., "Meander open complementary split ring resonator (MOCSRR) particles implemented using coplanar waveguides," *IEEE International Conference on Wireless Information Technology and Systems*, Honolulu, Hawaii, Aug. 28 - Sep. 3, 2010b.
- Cai, A.; Qing, X.; & Chen, Z.N., "High frequency RFID smart table antenna," *Microwave Optical Technological Letters*, vol. 49, no. 9, September 2007, pp. 2074-2076.
- Calabrese, C. & Marrocco, G., "Meander-slot antennas for sensor-RFID tags," *IEEE Antennas and Wireless Propagation Letters.*, vol. 7, pp. 5-8, 2008.
- Collin, R. E. (2001). *Foundations for Microwave Engineering*, 2<sup>nd</sup> ed., John Wiley and Sons, Inc. Hoboken, New Jersey.
- Dacuna, J. & Pous, R. "Miniaturized UHF tags based on metamaterials geometries," *Building Radio Frequency Identification for the Global Environment*, July 2007, [Online], [www.bridge-project.eu](http://www.bridge-project.eu).

- Eleftheriades, G. V. & Balmain, K. G. (2005) *Negative-Refractive Metamaterials: Fundamentals Principles and Applications*, John Wiley and Sons, Hoboken, New Jersey.
- Finkenzeller, K. (2003). *RFID Handbook: Fundamentals and Applications in Contactless Smart Cards and Identification*, John Wiley and Sons, West Sussex, England.
- Griffin, J.D.; Durgin, G.D.; Haldi, A.; & Kippelen, B., "RF tag antenna performance on various materials using radio link budgets," *IEEE Antennas and Propagation Letters*, vol. 5, no. 1, 2006, pp. 247-250.
- Jefflindsay, 2010, "RFID Systems for Enhanced Shopping Experiences," Experiences," <http://www.jefflindsay.com/rfid4.html>
- Kanan, R.; & Azizi, A., "UHF RFID transponders antenna design for metal and wood surfaces," *IEEE International Conference on RFID*, pp. 270-277, April, 2009, Orlando, FL.
- Landt, J., "The history of RFID," *IEEE potentials*, vol. 24, no. 4, 2005, pp. 8-11.
- Lee, J.M.; Kim, N.S.; & Pyo, C.S., "A circular polarized metallic patch antenna for RFID reader," in *Asia-Pacific Conference on Communication*, pp. 116-118, October 2005, Australia.
- Marrocco, G., "Gain-optimized self-resonant meander line antennas for RFID applications," *IEEE Antennas and Wireless Propagation Letters*, vol. 2, pp. 302-305, 2003.
- Medeiros, C.R.; Costa, J.R.; & Fernandes, C.A., "RFID smart shelf with confined detection volume at UHF," *IEEE Antennas and Wireless Propagation Letters*, vol. 7, 2008, pp. 773-776.
- Mohammed, N.A.; Sivakumar, M.; & Deavours, D.D., "An RFID tag capable of free-space and on-metal operation," *IEEE Radio and Wireless Symposium*, pp. 63-66, 2009, San Diego, CA.
- Ng, M. L.; Leong, K. S.; Hall, D.M.; & Cole, P.H., "A small passive UHF RFID tag for livestock identification," *IEEE International Symposium on Microwave, Antenna, Propagation and EMC Technologies for Wireless communications*, vol. 1, 2005, pp. 67-70.
- Pozar, D. M. (2005). *Microwave Engineering*, 3<sup>rd</sup> ed., John Wiley and Sons, Inc., Hoboken, New Jersey.
- Qing, X. & Chen, Z.N., "Proximity effects of metallic environments on high frequency RFID reader antenna: Study and Applications," *IEEE Transactions on Antennas and Propagation*, vol. 55, no. 11, November, 2007, pp. 3105-3111.
- Rao, K. V. S.; Nikitin, P.V.; & Lam, S.F., "Antenna Design for UHF RFID Tags: A Review and a Practical Application," *IEEE Transactions on Antennas and Propagation*, vol. 53, no. 12, December, 2005, pp. 3870-3876.
- Rao, K. V. S.; Nikitin, P.V.; & Lam, S.F., "Wideband metal mount UHF RFID tag," *IEEE Antenna and Propagation Society International Symposium*, pp. 1-4, 2008, San Diego, CA.
- Stutzman, W.L. & Thiele, G.A. (1998). *Antenna Theory and Design*, 2nd ed., John Wiley and Sons, Inc., New York.
- Teco, 2010, "RFID Smart Shelf," <http://www.teco.edu/research/projects/smartshelf/>.
- Velez, A.; Aznar, F.; Bonache, J.; Valazquez-Ahumada, M. C.; Martel, J.; and Martin, F., "Open complementary split ring resonators (OCSRRs) and their application to

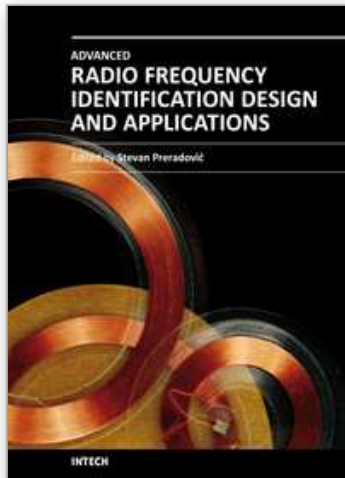
wideband CPW band pass filter," *IEEE Microwave and Wireless Components Letters*, vol. 19, no. 4, pp. 197-199, Apr. 2009.

Want, R., "An introduction to RFID technology," *IEEE Pervasive Computing*, vol. 5, no. 1, 2006, pp. 25-33.

Zhu, W.; Yuan, B.; Zhang, Z.; Wang, J.; & Huang, J., "A novel 2.4 GHz Quasi-Yagi tag antenna for RFID of metallic object," *Asia Pacific Microwave Conference*, pp. 1-4, 2008, Macau.

IntechOpen

IntechOpen



## **Advanced Radio Frequency Identification Design and Applications**

Edited by Dr Stevan Preradovic

ISBN 978-953-307-168-8

Hard cover, 282 pages

**Publisher** InTech

**Published online** 22, March, 2011

**Published in print edition** March, 2011

Radio Frequency Identification (RFID) is a modern wireless data transmission and reception technique for applications including automatic identification, asset tracking and security surveillance. This book focuses on the advances in RFID tag antenna and ASIC design, novel chipless RFID tag design, security protocol enhancements along with some novel applications of RFID.

### **How to reference**

In order to correctly reference this scholarly work, feel free to copy and paste the following:

Benjamin D. Braaten and Masud A. Aziz (2011). Using Metamaterial-Based Coplanar Waveguide Structures for the Design of Antennas on Passive UHF RFID Tags, *Advanced Radio Frequency Identification Design and Applications*, Dr Stevan Preradovic (Ed.), ISBN: 978-953-307-168-8, InTech, Available from: <http://www.intechopen.com/books/advanced-radio-frequency-identification-design-and-applications/using-metamaterial-based-coplanar-waveguide-structures-for-the-design-of-antennas-on-passive-uhf-rfi>

**INTECH**  
open science | open minds

### **InTech Europe**

University Campus STeP Ri  
Slavka Krautzeka 83/A  
51000 Rijeka, Croatia  
Phone: +385 (51) 770 447  
Fax: +385 (51) 686 166  
[www.intechopen.com](http://www.intechopen.com)

### **InTech China**

Unit 405, Office Block, Hotel Equatorial Shanghai  
No.65, Yan An Road (West), Shanghai, 200040, China  
中国上海市延安西路65号上海国际贵都大饭店办公楼405单元  
Phone: +86-21-62489820  
Fax: +86-21-62489821

© 2011 The Author(s). Licensee IntechOpen. This chapter is distributed under the terms of the [Creative Commons Attribution-NonCommercial-ShareAlike-3.0 License](#), which permits use, distribution and reproduction for non-commercial purposes, provided the original is properly cited and derivative works building on this content are distributed under the same license.

IntechOpen

IntechOpen